High strength and ductility aluminium alloy processed by high pressure die casting

Xixi Dong[a], Hailin Yang[b], Xiangzhen Zhu[a], Shouxun Ji [a,*]

[a] Brunel Centre for Advanced Solidification Technology (BAST), Institute of Materials and Manufacturing, Brunel University London, Uxbridge UB8 3PH, United Kingdom

[b] State Key Laboratory of Powder Metallurgy, Central South University, Changsha 410083, China

[*]Corresponding author: Tel: +44 1895 266663; Fax: +44 1895 269758

E–mail address: shouxun.ji@brunel.ac.uk

Abstract

A high strength (Yield strength ≥ 320 MPa) and high ductility (Tensile elongation ≥ 10 %) die–cast aluminium alloy was first developed. The AlSiCuMgMn alloy processed by high pressure die casting can provide the high yield strength of 321 MPa, the high ultimate tensile strength of 425 MPa and the high ductility of 11.3 %, after solution treated at 510 °C for 30 min and aged at 170 °C for 12 h. The alloy demonstrated 150 % increase in ductility over the reported most advanced die–cast aluminium alloy, also comparable tensile properties to the 6000 series wrought aluminium alloys but with much lower manufacturing cost. The as–cast microstructure of the alloy mainly contained the primary α_1–Al phase solidified in the shot sleeve, the secondary α_2–Al phase solidified in the die, the Al–Si eutectic phase and the intermetallic phases Q–$Al_5Cu_2Mg_8Si_6$ and θ–Al_2Cu. The intermetallic phases Q and θ were dissolved into the α–Al matrix during solution. Nanoscale precipitates Q' and θ' were precipitated from the α–Al matrix for the strengthening of the alloy through ageing treatment. Multiple effects resulted in the high ductility of the alloy.

Key words: Aluminium alloy; High pressure die casting; High strength; High ductility.

1. Introduction

High pressure die casting (HPDC) is a near–net shape manufacturing process in which molten metal is injected into a metal mould at high speed and solidified under high pressure. HPDC has been widely used in producing thin wall aluminium and magnesium alloy components with high dimensional accuracy, high production efficiency, and considerable economic benefit for automotive and other industries [1–5]. However, the turbulent flow and the consequent entrapment of air during die filling is an inherent problem for HPDC, which results in the formation of gas porosity in HPDC castings [6–8]. The presentence of gas porosity decreases the possibility of the further strengthening of HPDC castings through heat treatment due to blistering. Therefore, the application of HPDC is normally limited to low strength as–cast non–structural components not requiring heat treatment for strengthening.

Recent development in manufacturing lightweight components requires the die–cast aluminium alloys to be able to provide higher strength and high ductility. High strength and high ductility (Yield strength ≥ 320 MPa, Elongation ≥ 10 %) die–cast aluminium alloys are attractive in industry, because they are comparable with the tensile properties of 6000 series wrought aluminium alloys [9–12], but with much lower manufacturing cost. The problem is that the as–cast tensile properties of the currently available die–cast aluminium alloys are usually low, with a yield strength of 130~170 MPa and an elongation of 3~5 % [13]. Explorations were done to develop die–cast aluminium alloys with higher as–cast strength [14–18]. Hu et al. [14] reported a die–cast Al–Mg–Si–Mn alloy with a yield strength of 183 MPa. Zhang et al. [15] developed an Al–5Mg–0.6Mn die–cast alloy with a yield strength of 212 MPa. However, the as–cast yield strength of the currently developed die–cast aluminium alloys is still around the low level of 200 MPa [15,18].

The successful development of the vacuum assisted HPDC has provided the capability of producing castings with much reduced gas porosities, which enables the further strengthening of the as–cast heat treatable die–cast alloys through heat treatment [19–24]. Ji et al. [13,25] developed a high strength Al–10Mg–3.5Zn–3Si die–cast alloy exhibited the yield strength of 320 MPa, the UTS of 420 MPa and the tensile elongation of 4.5 % after solution and ageing heat treatment. The tensile elongation of 4.5 % was the highest reported ductility in association with a high yield strength of 320 MPa for die–cast aluminium alloys processed by HPDC. Die–cast aluminium alloy with both high yield strength above 320 MPa and high ductility over 10 % is still unachievable.

The objective of the present work is to develop a die–cast aluminium alloy to achieve the high yield strength above 320 MPa and the high ductility over 10 %. HPDC was applied for the processing of the alloy. The microstructure, mechanical properties and the strengthening mechanism of the alloy under as–cast and heat treatment condition were investigated.

2. Experimental

2.1. Materials and melt preparation

The AlSiCuMgMn die–cast alloy, with the actual composition of 8.82wt.%Si, 1.71wt.%Cu, 0.40wt.%Mg, 0.50wt.%Mn, 0.18wt.%Fe, 0.13wt.%Ti and balanced Al, was melted in a 15–kg capacity clay–graphite crucible using an electric resistance furnace. During melting, the temperature of the furnace was controlled at 750 °C, and a melt of 10 kg was prepared. The melt was held for one hour to ensure the good homogenisation of the composition, since the melt was prepared based on the addition and melting of pure Al, pure Mg and Al–50 wt.% Si, Al–50 wt.% Cu, Al–20 wt.% Mn, Al–45 wt.% Fe and Al–10 wt.% Ti master alloys. The activated element Mg was over added by 5 % to compensate its burning loss during the holding of the melt. After one hour of homogenisation, Al–10 wt.% Sr master alloy was added into the melt to make the defined Sr content of 200 ppm, for modifying the morphology of the eutectic silicon phase during solidification. The melt was then degassed through injecting pure argon into the melt by using a rotary degassing impeller at a speed of 350 rpm for 5 min. After degassing, the melt was covered by the commercial granular flux, and the melt was hold for 10 min for temperature recovery, followed by the HPDC.

2.2. High pressure die casting

A 4500 kN cold chamber HPDC machine was applied for the present HPDC, as shown in Fig. 1(a). Fig. 1(b) shows the die–set in the cold chamber HPDC machine. The casting die was heated by the circulation of mineral oil at 120 °C, and the shot sleeve was heated by the circulation of compressed hot water. The prepared AlSiCuMgMn alloy melt was loaded into the shot sleeve for HPDC. The pouring temperature of melt was controlled exactly at 690 °C measuring by the K–type thermocouple. Eight ASTM B557 standard round tensile test bars with a gauge dimension of ϕ6.35 mm × 50 mm were casted under each HPDC shot, as shown in Fig. 1(c).

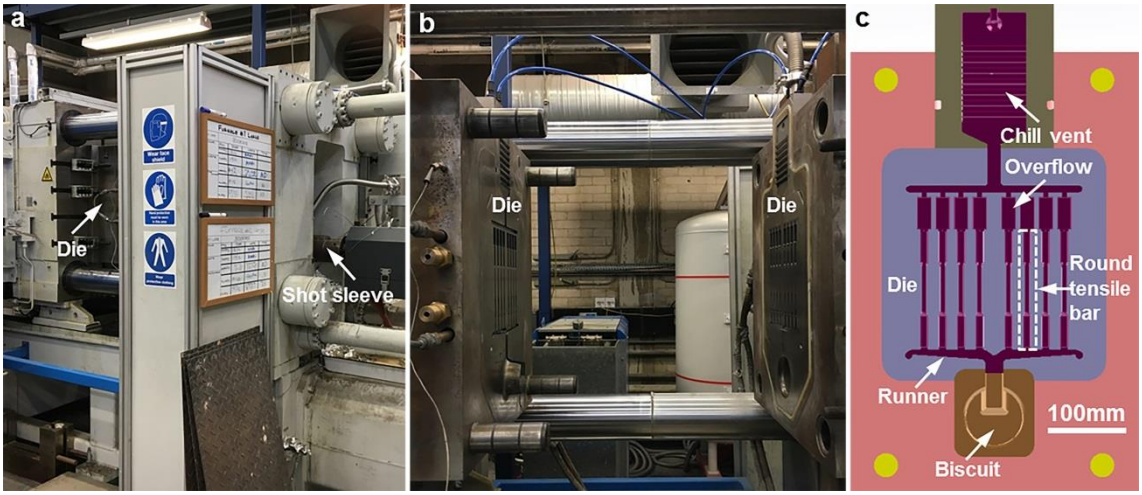

Fig. 1. (a) Cold chamber high pressure die casting machine and (b) die–set in the machine, and (c) cross section of die–set showing the round tensile test bars casted by the die.

2.3. Heat treatment and mechanical properties tests

After kept at ambient condition for at least 24 h, the as–cast tensile test bars processed by HPDC were subjected to T6 heat treatment in an electrical furnace equipped with forced air circulation, including solution treatment and subsequent artificial ageing. Solution treatment was carried out at 510 °C for 30 min, followed by immediate water quenching to room temperature. Ageing treatment was performed at 170 °C for 12 h, followed by air cooling to room temperature. Tensile tests were conducted at room temperature following the ASTM standard using an Instron 5500 Universal Electromechanical Testing System. The gauge length of the extensometer was 50 mm and the ramp rate for extension was 1 mm/min. Each tensile data reported with standard deviation was based on the testing of at least six samples. Vickers hardness test was conducted on a FM–800 hardness tester with an applied load of 10 kg for 10 s, and 10 to 12 measurements were performed for each sample with the average reported as the hardness.

2.4. Microstructure characterization

The specimens for microstructure characterization were cut from the middle of ϕ6.35 mm round tensile test bars. The microstructure was examined using the Zeiss optical microscopy (OM), the Zeiss SUPRA 35VP scanning electron microscope (SEM) equipped with energy dispersive X–ray spectroscopy (EDS) and the JEOL–2100 transmission electron microscopy (TEM). The specimens for OM and SEM analysis were prepared by the standard technique of grinding. Polarized OM observation was performed after anodised with Barker solution (97 vol.% H_2O and 3 vol.% HBF_4). SEM analysis was conducted after etching with 15 vol.% HCl. Post–loading fracture analysis was also performed via SEM. Thin specimens for TEM observation were prepared by standard electropolishing. The electrolytic solution was a mixture of nitric acid and methyl alcohol (2:8), used at –20 to –30 ℃ and 20 V. TEM operating at 200 kV was used for bright field imaging, select area diffraction pattern (SADP) analysis, and high–resolution transmission electron microscopy (HRTEM) imaging.

3. Results & discussion

3.1. Microstructure

3.1.1. OM microstructure

Fig. 2(a) shows the polarized optical micrograph of the as–cast AlSiCuMgMn alloy processed by HPDC. Two kinds of α–Al phase with different size were found in the as–cast

alloy, i.e., the primary α_1–Al phase solidified in the shot sleeve and the secondary α_2–Al phase solidified in the die cavity. The size of the α_2–Al phase is much finer than that of the α_1–Al phase, due to the higher cooling rate in the die cavity. Figs. 2(b), (c) and (d) show the polarized optical micrographs of the AlSiCuMgMn alloy processed by HPDC after solution treated at 510 °C for 0.5h, 1h and 2h, respectively. The α_1–Al phase and the α_2–Al phase were also present in the alloy after solution treatment, but the α_1–Al phase and the α_2–Al phase in the solution treated alloy were observed coarsening gradually with increasing solution time, when compared with that in the as–cast alloy. The coarsening of the α–Al phase during solution treatment was due to the high temperature diffusion and the growth and merging of α–Al grains. Solution at 510 °C for 0.5h was found enough for the good spheroidisation of the eutectic Si phase and the solid solution of the intermetallic phases in Section 3.1.3 and 3.1.4, and longer solution time will increase the risks of grain coarsening and blistering, so 0.5h was chosen as the solution time for the present alloy.

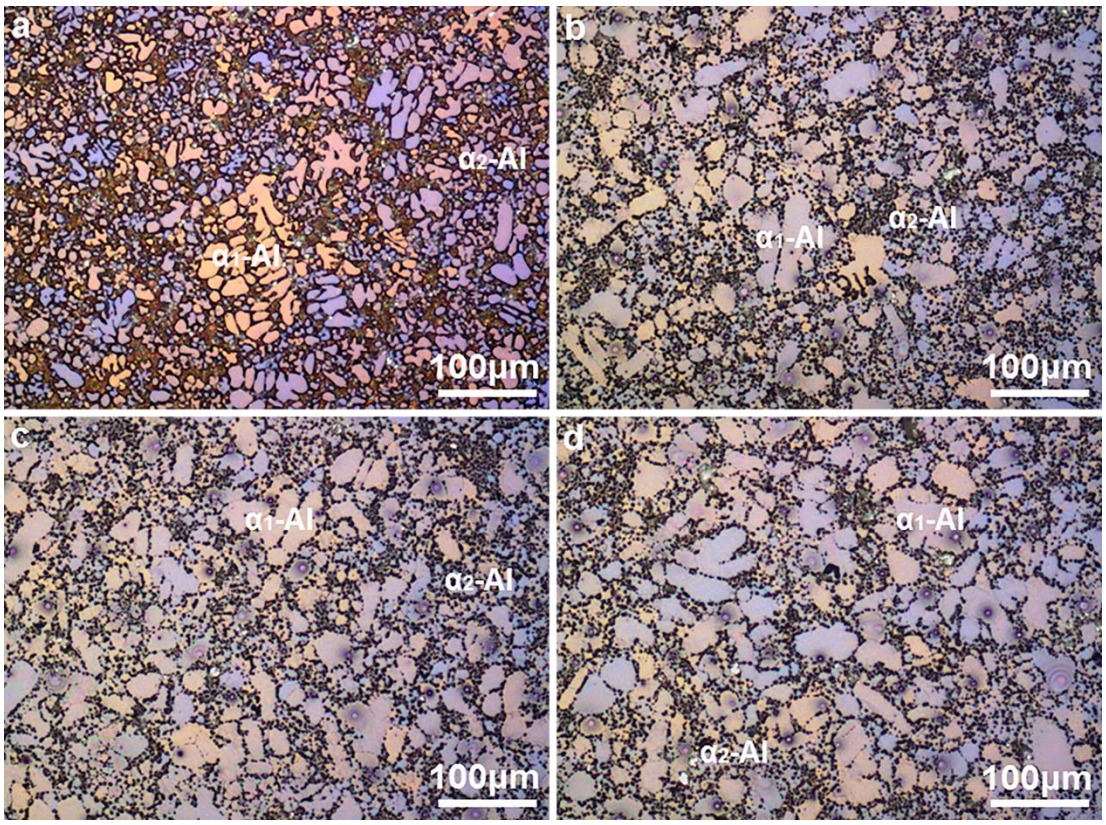

Fig. 2. Polarized optical micrographs showing the primary α_1-Al phase nucleated in the shot sleeve and the secondary α_2-Al phase nucleated in the die cavity in the AlSiCuMgMn alloy processed by high pressure die casting: (a) as–cast, (b) solution at 510 °C for 0.5h, (c) solution at 510 °C for 1h and (d) solution at 510 °C for 2h.

3.1.2. As–cast SEM microstructure

Fig. 3(a) and Fig. 3(b) show the low magnification and high magnification SEM morphology of the as–cast AlSiCuMgMn alloy processed by HPDC, respectively. From Fig. 3(a), the α_1–Al phase and the α_2–Al phase were also observed in the as–cast alloy under SEM. From Fig. 3(b), Al–Si eutectic phase and the Cu–containing intermetallic phases Q–$Al_5Cu_2Mg_8Si_6$ and θ–Al_2Cu were also identified in the as–cast alloy. The eutectic Si phase was properly modified to the fine fibrous structure by the addition of Sr [26,27]. It has been well reported and confirmed by literatures that Q–$Al_5Cu_2Mg_8Si_6$ phase and θ–Al_2Cu phase

are the only two Cu-containing intermetallic phases always present in the gravity cast and die-casting Al–Si–Cu–Mg alloys [24,28,29]. The EDS results of the two intermetallic phases present in the present alloy agreed with the reported Q–$Al_5Cu_2Mg_8Si_6$ phase and θ–Al_2Cu phase in atomic ratio, which confirm the existence of the Q–$Al_5Cu_2Mg_8Si_6$ and θ–Al_2Cu intermetallic phases in the present alloy, as shown in Figs. 3(c) and (d). The intermetallic phases Q and θ mainly distribute in the grain boundary and near the Al–Si eutectic area.

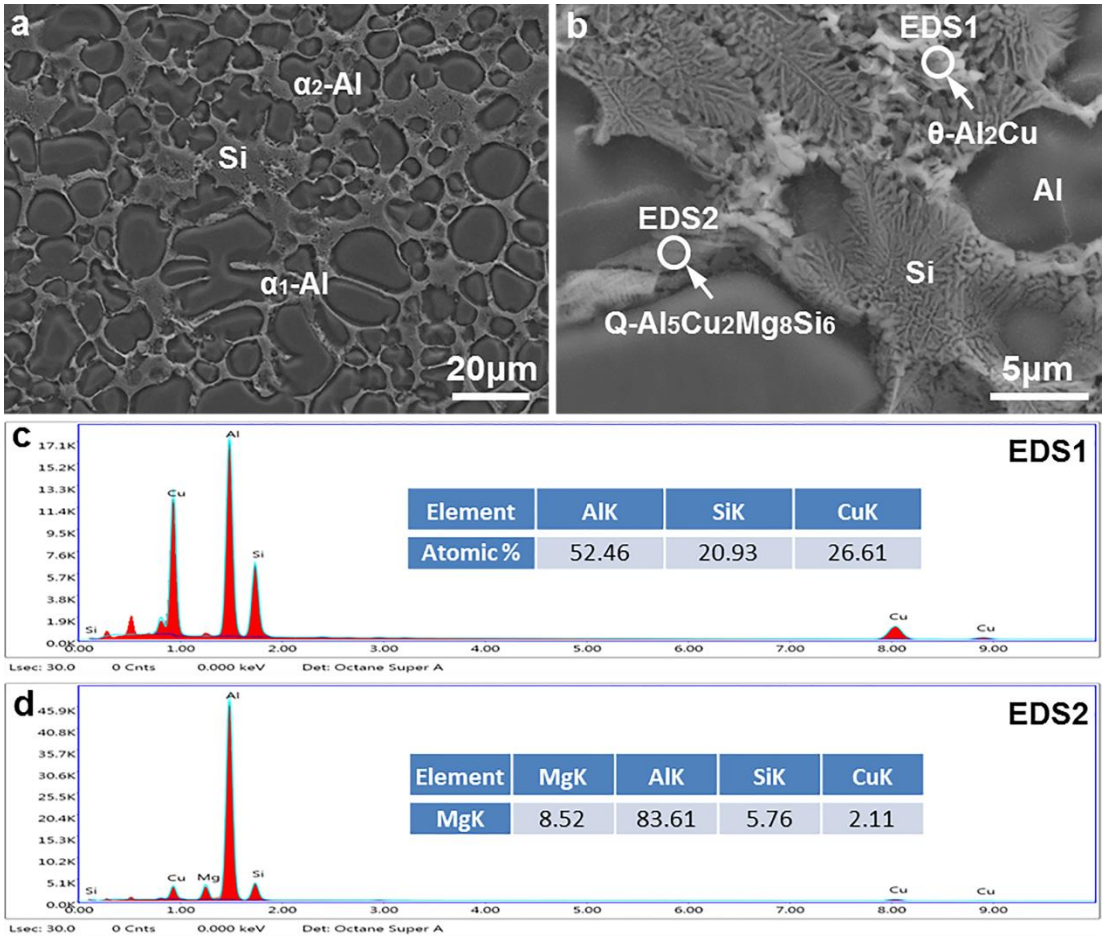

Fig. 3. SEM micrographs showing (a,b) the morphology of different phases, (c) EDS of θ phase and (d) EDS of Q phase of the as–cast AlSiCuMgMn alloy processed by high pressure die casting.

3.1.3. SEM microstructure after heat treatment

Fig. 4(a) and Fig. 4(b) show the low magnification and high magnification SEM morphology of the AlSiCuMgMn alloy processed by HPDC, separately, after T6 heat treatment. From Fig. 4(a), the α_1–Al phase and the α_2–Al phase were still in the alloy after T6 heat treatment. From Fig. 4(b), the eutectic Si phase was changed into the spheroidal morphology. The EDS result in Fig. 4(c) verifies that the spheroidal phase is the Si phase. The spheroidisation of the Si phase is attributed to the solution heat treatment, and it is beneficial to the mechanical properties especially ductility [26]. In addition, the intermetallic phases Q–$Al_5Cu_2Mg_8Si_6$ and θ–Al_2Cu were hardly observed in the T6 heat–treated microstructure, which indicated that the intermetallic phases Q–$Al_5Cu_2Mg_8Si_6$ and θ–Al_2Cu were well dissolved into the α–Al matrix after the solution treatment. The well solution of intermetallic phases Q–$Al_5Cu_2Mg_8Si_6$ and θ–Al_2Cu could result in the precipitation of nanoscale strengthening precipitates in the α–Al matrix after ageing treatment, which contributes to the precipitation strengthening of the alloy after T6 heat treatment.

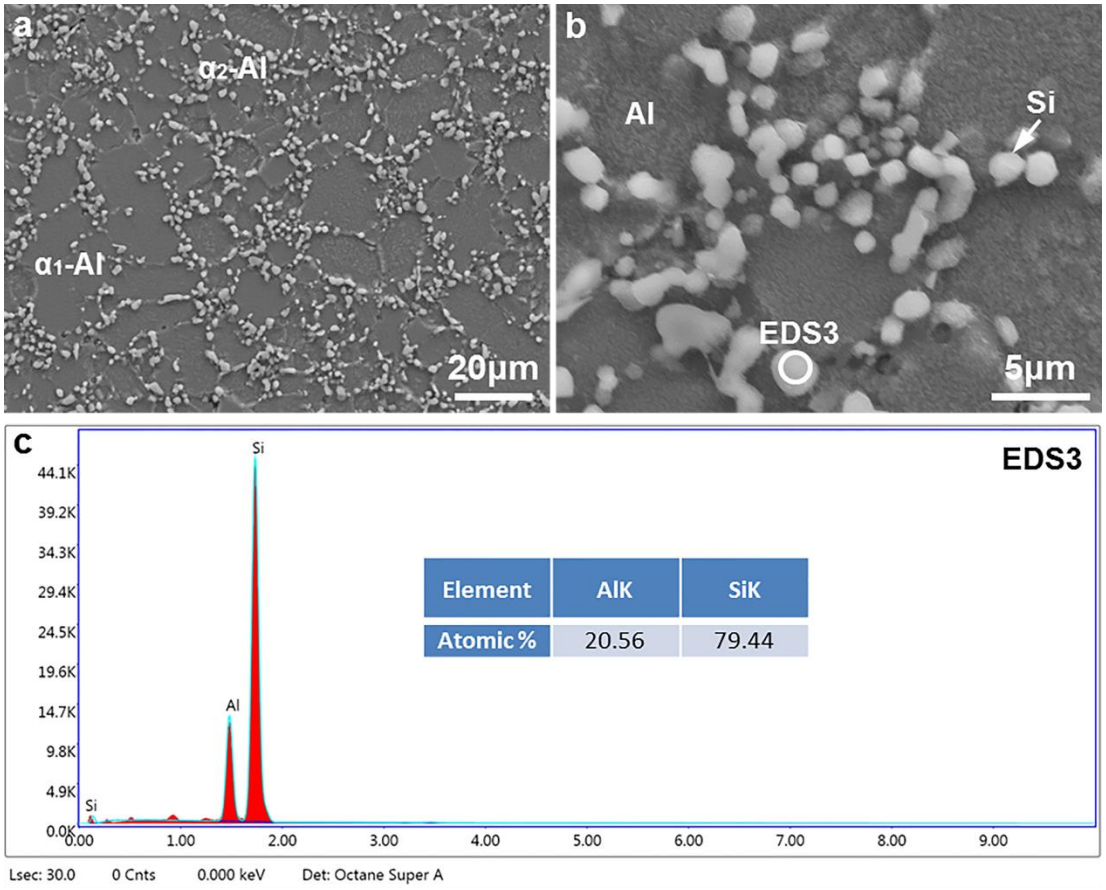

Fig. 4. SEM micrographs showing (a,b) the morphology of different phases and (c) EDS of Si phase of the AlSiCuMgMn alloy processed by high pressure die casting after T6 heat treatment.

3.1.4. Solid solution effect

Figs. 5(a) and (c) show the EDS result of the alloying element solution into the Al matrix of the as–cast AlSiCuMgMn alloy. The amounts of the Mg and Cu elements solution into the Al matrix of the as–cast alloy were 0.28 wt.% and 0.33wt.%. Figs. 5(b) and (d) show the EDS result of the alloying element solution into the Al matrix of the AlSiCuMgMn alloy after solution treated at 510 °C for 0.5h. The amounts of the Mg and Cu elements solution into the Al matrix of the solution treated alloy increased to 0.38 wt.% and 1.62 wt.%, which were close to the full amounts of 0.40 wt.% Mg and 1.71 wt.% Cu in the alloy, indicating the well dissolving of the intermetallic phases Q and θ after solution at 510 °C for 0.5h. From Figs. 5(c) and (d), the amount of Si solution into the Al matrix of the alloy kept nearly the same (~1.4 wt.%) before and after solution treatment, indicating that the spheroidisation of the eutectic Si phase happened in-situ in the grain boundary and no dissolving of Si into the Al matrix during solution treatment. It should be mentioned that the EDS analysis in Fig. 5 was conducted on the samples without etching to give accurate EDS results.

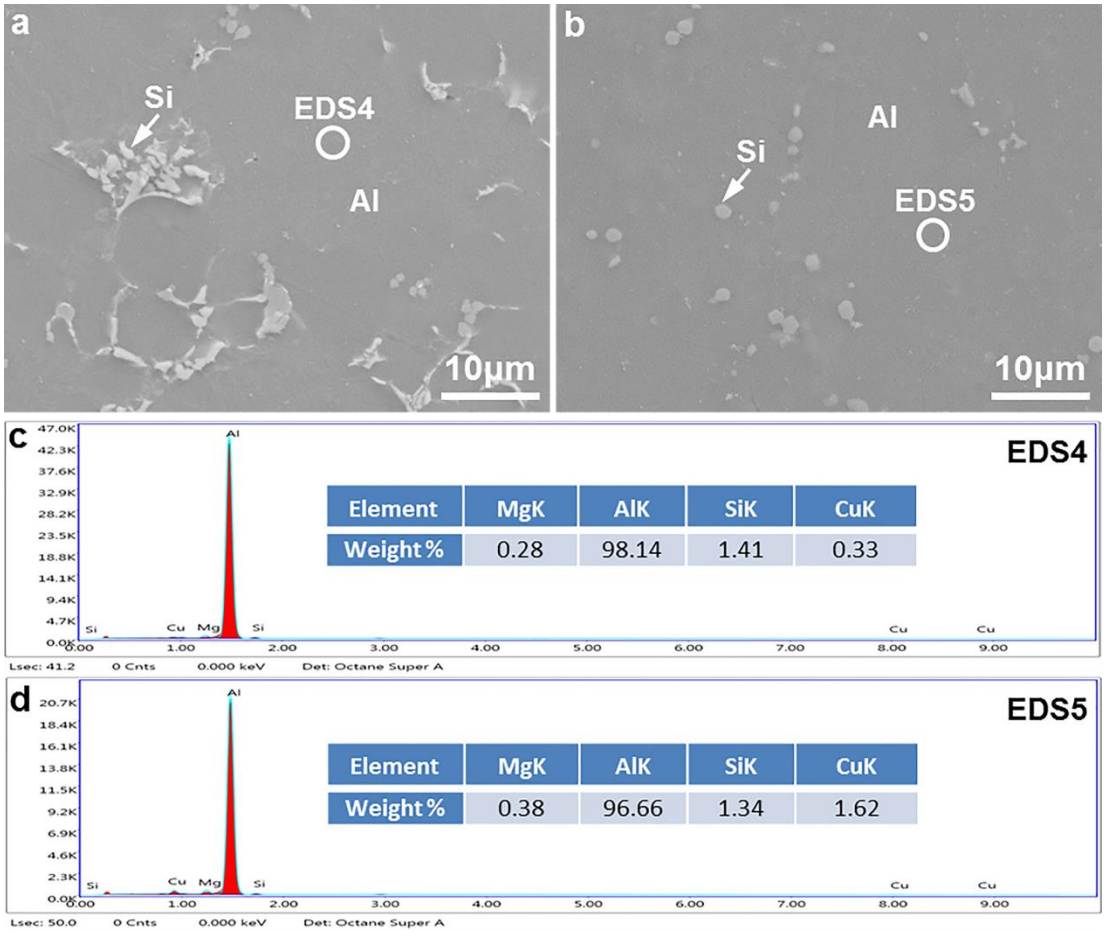

Fig. 5. SEM results showing the solid solution of alloying elements in the AlSiCuMgMn alloy processed by high pressure die casting: (a,c) as–cast and (b,d) after solution treated at 510 °C for 0.5h.

3.2. Mechanical properties

3.2.1. As–cast tensile properties

Fig. 6(a) shows the tensile stress–strain curves of the as–cast AlSiCuMgMn alloy processed by HPDC. The as–cast AlSiCuMgMn alloy processed by HPDC has strong strain strengthening effect, with a strain strengthening of ~ 180 MPa during the plastic deformation stage. The impediment of the grain boundary sliding by the intermetallic phases in the grain boundary contributes to the significant strain strengthening of the as–cast alloy. Fig. 6(b) shows the tensile properties of the as–cast AlSiCuMgMn alloy processed by HPDC. The yield strength, UTS and elongation of the as–cast alloy processed by HPDC are 189.1±3.7 MPa, 372.2±5.5 MPa and 8.0±1.1 %, respectively. The UTS of the as–cast AlSiCuMgMn alloy is superior to the currently reported advanced die–cast aluminium alloys [14–18].

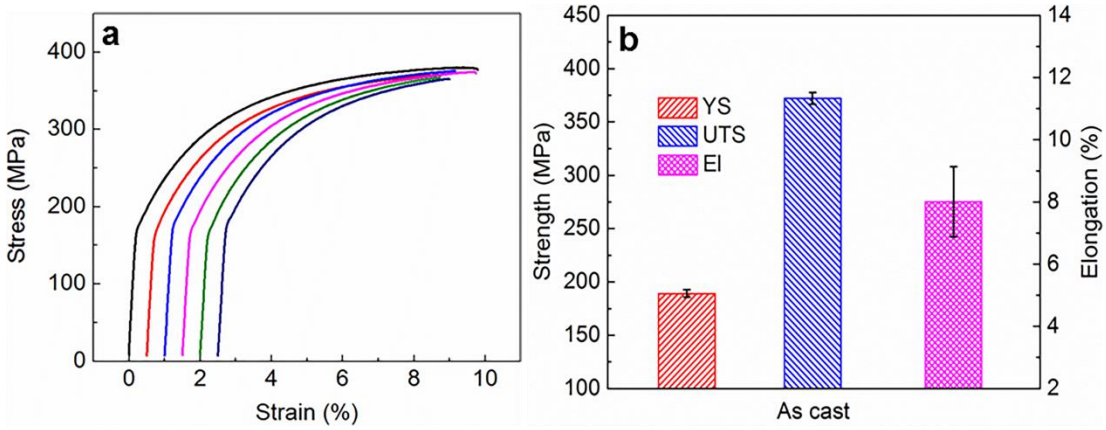

Fig. 6. (a) Tensile stress–strain curves and (b) tensile properties of the as–cast AlSiCuMgMn alloy processed by high pressure die casting.

3.2.2. Tensile properties after solution heat treatment

Fig. 7(a) shows the tensile stress–strain curves of the AlSiCuMgMn alloy processed by HPDC, after T4 heat treatment, i.e., solution treated at 510 °C for 0.5h and followed by water quench. Fig. 7(b) shows the tensile properties of the alloy after T4 heat treatment. The yield strength, UTS and elongation of the T4 heat–treated alloy are 210.8±2.1 MPa, 390.8±3.9 MPa and 20.7±0.7 %, respectively. The yield strength of the T4 heat–treated alloy is 21.7 MPa higher than that of the as–cast alloy due to solution strengthening. The T4 heat–treated alloy has similar strong strain strengthening of 180 MPa to the as–cast alloy. Compared with the as–cast alloy, the ductility of the T4 heat–treated alloy is improved significantly by 159 %, due to the well solution of the intermetallic phases in the grain boundary into the matrix and the in-situ spheroidisation of the eutectic Si phase in the grain boundary.

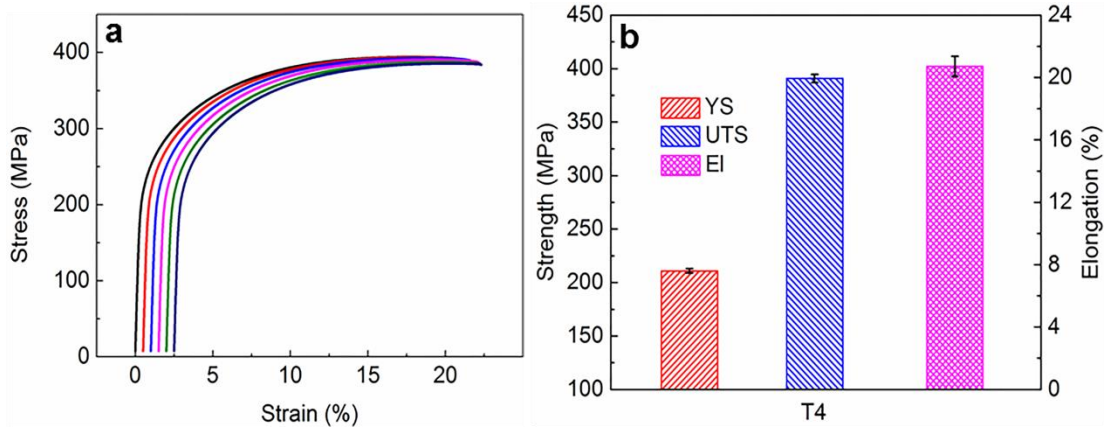

Fig. 7. (a) Tensile stress–strain curves and (b) tensile properties of the AlSiCuMgMn alloy processed by high pressure die casting after T4 heat treatment.

3.2.3. Evolution of ageing hardness

Fig. 8 shows the evolution of the Vickers hardness (HV) of the AlSiCuMgMn alloy processed by HPDC versus ageing time at an ageing temperature of 170 °C, after solution at 510 °C for 30 min. The hardness of the AlSiCuMgMn alloy first increases sharply with ageing time till 4 h, then increases slightly with ageing time till reaching the highest peak at 12 h, subsequently decreases to the valley at 14 h and increases again to the secondary peak at 16 h, after decreases again. The increase of hardness is attributed to the precipitation of the metastable precipitates, and the decrease of hardness results from the transformation of

metastable precipitates to stable precipitates. The metastable precipitates are coherent with the Al matrix and have the strongest strengthening effect, while the stable precipitates are not coherent with the Al matrix and have much weaker strengthening effect.

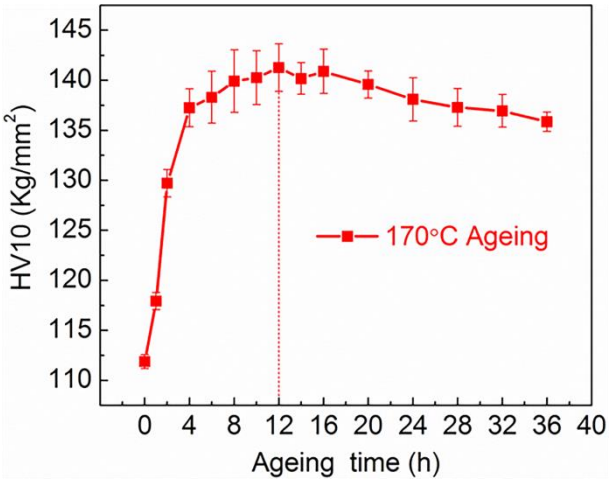

Fig.8. Evolution of the hardness (HV) of the AlSiCuMgMn alloy processed by high pressure die casting versus ageing time after solution treated at 510 °C for 30 min.

3.2.4. Tensile properties after solution and ageing treatment

Fig. 9(a) shows the tensile stress–strain curves of the AlSiCuMgMn alloy processed by HPDC, after T6 heat treatment, i.e., solution treated at 510 °C for 30 min and peak ageing treated at 170 °C for 12 h, and all the descriptions of T6 heat treatment in the text mean the same solution and ageing specification. The strength and the ductility of the T6 heat–treated AlSiCuMgMn alloy is significantly higher than that of the as–cast alloy, while the strain strengthening of ~ 100 MPa during the plastic deformation stage of the T6 heat–treated alloy is weaker than that of the as–cast alloy. The precipitation strengthening results in the increase of strength in the T6 heat–treated alloy, and the spheroidization of the Si phase and the well solution of the intermetallic phases lead to the increase of ductility in the T6 heat–treated alloy. According to Section 3.2.2, the strain strengthening (~180MPa) of the alloy after solution treatment was the same as that of the as–cast alloy, but the eutectic Si phase in the grain boundary was changed and the intermetallic phases in the grain boundary were well dissolved into the Al matrix after solution treatment, when compared with the as–cast condition. Thus the change of the eutectic Si phase and the dissolving of the intermetallic phases in the grain boundary during solution treatment do not play an important role for the change of the strain strengthening of the alloy, and the decrease of the strain strengthening to ~100MPa in the T6 heat–treated alloy was mainly attributed to the decrease of the strain strengthening capability of the Al matrix by the precipitation strengthening of the Al matrix after ageing treatment.

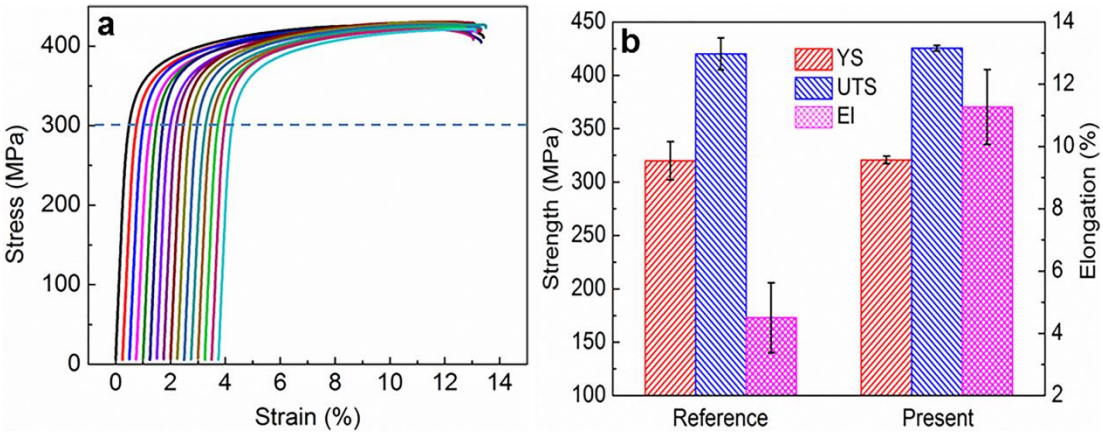

Fig. 9. (a) Tensile stress–strain curves and (b) tensile properties of the AlSiCuMgMn alloy processed by high pressure die casting after T6 heat treatment. Reference [25] was the reported die–cast aluminium alloy with the most advanced tensile properties.

Fig. 9(b) shows the tensile properties of the AlSiCuMgMn alloy processed by HPDC, after T6 heat treatment. The T6 heat–treated AlSiCuMgMn alloy has high yield strength of 320.7±3.5 MPa, high UTS of 425.4±2.6 MPa and high ductility of 11.3±1.2 %. The reported die–cast aluminium alloy with the most advanced tensile properties was the Al–10Mg–3.5Zn–3Si alloy, which exhibited the yield strength of 320±18 MPa, the UTS of 420±15 MPa and the elongation of 4.5±1.1 %, and it was chosen as the reference [25] in comparison with the present alloy, see Fig. 9(b). The yield strength and UTS of the present AlSiCuMgMn alloy are slightly higher than that of the reference alloy, but the fluctuations of the yield strength and UTS of the present alloy are significantly lower than that of the reference alloy, with the standard deviations of the yield strength and UTS that are only 19.4 % and 17.3 % of the reference alloy, respectively. The present alloy has more stable strength than the reference alloy. In addition, the elongation of the present alloy is significantly higher than that of the reference alloy, with the increase of elongation by 150 % over the reference alloy.

3.3. Precipitate strengthening

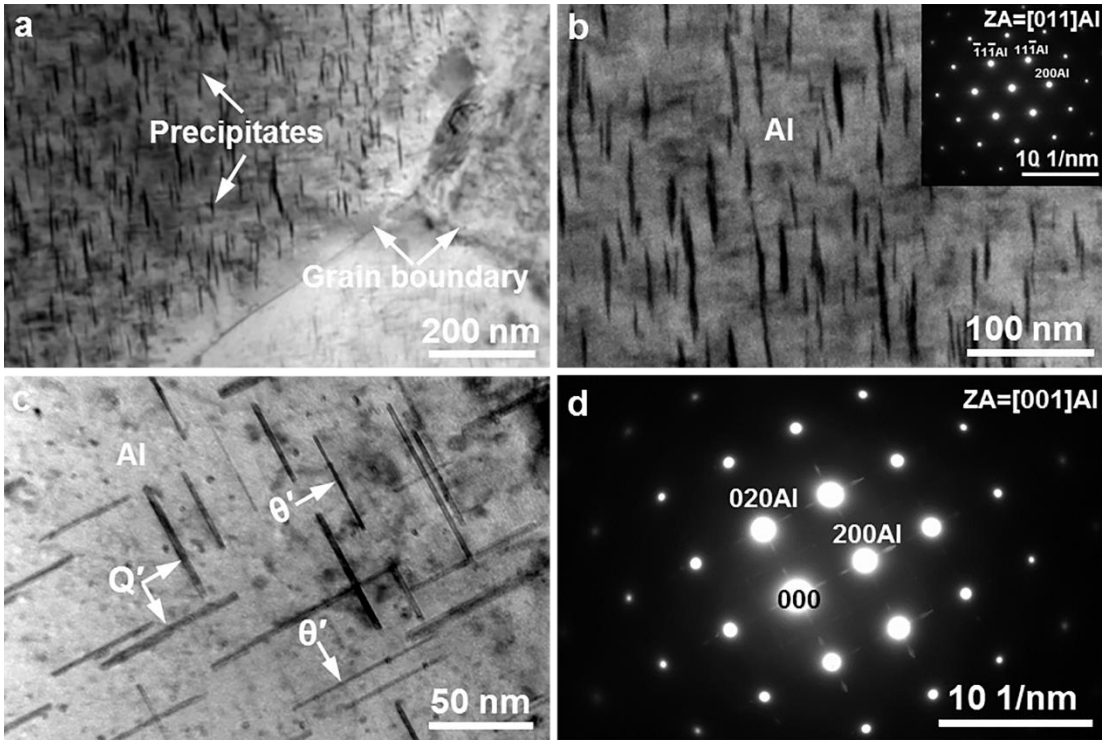

Fig. 10. TEM images taken along (a,b) <011>$_{Al}$ axis and (c,d) <001>$_{Al}$ axis showing the precipitation strengthening of the AlSiCuMgMn alloy processed by high pressure die casting after T6 heat treatment, (a,b,c) bright field image of precipitates, (d) SADP of (c).

Fig. 10(a) and Fig. 10(b) present the bright field TEM micrographs taken along the <011>$_{Al}$ axis showing the precipitate strengthening in the AlSiCuMgMn alloy processed by HPDC, after T6 heat treatment. Nanoscale precipitates with high number density were observed precipitated from the interior of α–Al grains, for the strengthening of the α–Al matrix. Fig. 10(c) shows the bright field TEM micrograph taken along the <001>$_{Al}$ axis showing the precipitates in the AlSiCuMgMn alloy processed by HPDC, after T6 heat treatment. Fig. 10(d) shows the SADP of Fig. 10(c). Q' and θ' precipitates were identified coexisting in the α–Al matrix by EDS analysis, and HRTEM imaging and FFT patterns shown in Fig. 11. Cu, Mg and Si were included in the Q' precipitate, while only Cu was included in the θ' precipitate, under EDS analysis. In addition, the Q' precipitate has a larger thickness than the θ' precipitate, and these two precipitates can be easily distinguished in bright field TEM image by thickness, as indicated by the arrows in Fig. 10(c).

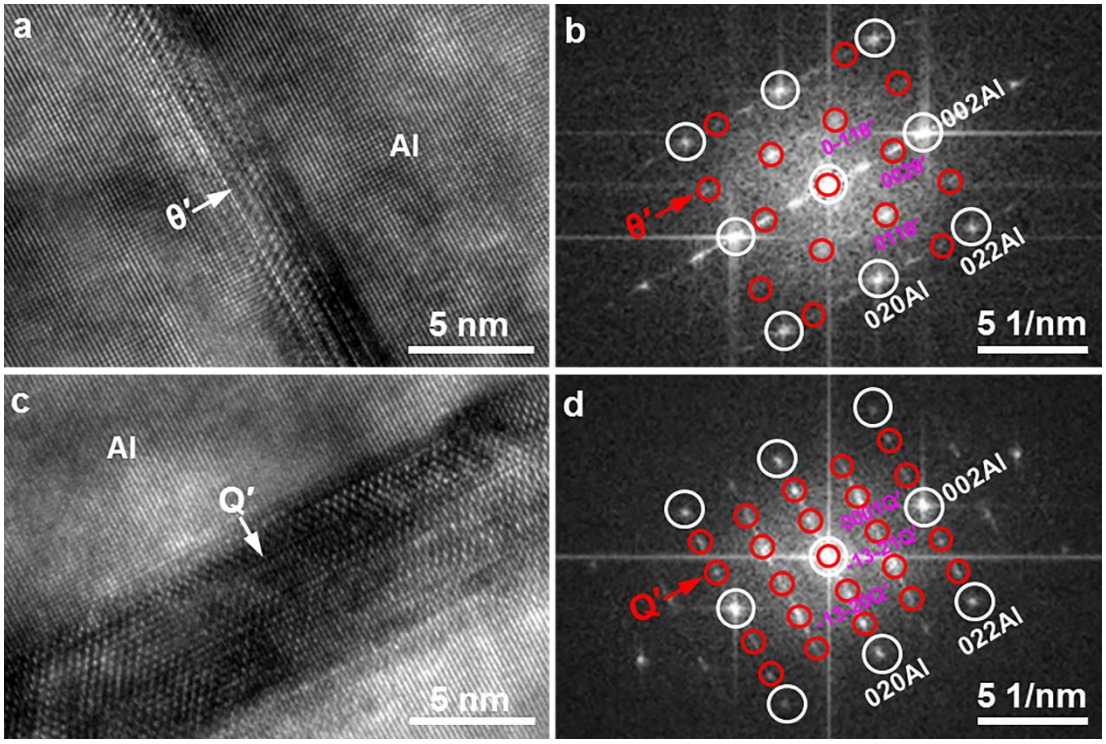

Fig. 11. HRTEM images taken along <001>$_{Al}$ axis showing the (a,b) θ′ precipitate and (c,d) Q′ precipitate in the AlSiCuMgMn alloy processed by high pressure die casting after T6 heat treatment, (b) FFT pattern of (a), (d) FFT pattern of (c). The θ′ orientation relationship is (001)Al//(001)θ′, [100]Al//[100]θ′. The Q′ orientation relationship is (001)Al//(0001)Q′, [100]Al//[51-40]Q′.

Fig. 11(a) presents the HRTEM image taken along the <001>$_{Al}$ axis showing the θ' precipitate in the AlSiCuMgMn alloy processed by HPDC, after T6 heat treatment. Fig. 11(b) shows the fast Fourier transform (FFT) pattern of Fig. 11(a), and the FFT pattern is consistent with the reported FFT pattern of the θ' precipitate [24,28,30], in addition, only Cu was included in the precipitate by EDS analysis, and these results verify that the precipitate shown in Fig. 11(a) is the θ' precipitate. The orientation relationship between the matrix and the θ' precipitate was indexed as (001)Al//(001)θ′ and [100]Al//[100]θ′, as shown in Fig. 11(b). Fig. 11(c) presents the HRTEM image taken along the <001>$_{Al}$ axis showing the Q' precipitate in the AlSiCuMgMn alloy processed by HPDC, after T6 heat treatment. Fig. 11(d) shows the FFT pattern of Fig. 11(c), and the FFT pattern is consistent with the reported FFT pattern of the Q' precipitate [24,28,30], in addition, Cu, Mg and Si were included in the precipitate by EDS analysis, and these results verify that the precipitate shown in Fig. 11(c) is the Q' precipitate. The orientation relationship between the matrix and the Q' precipitate was indexed as (001)Al//(0001)Q′ and [100]Al//[51-40]Q′, as shown in Fig. 11(d).

It is well known that the Al–Si–Cu alloy is mainly strengthened by the θ' precipitate after T6 heat treatment. The cooperative strengthening of the Al–Si–Cu alloy by the Q' and θ' precipitates with Mg present was reported by Hwang et al. [29]. Yang et al. [24] also found the cooperative strengthening of the Al–9Si–3.5Cu–Mg die–cast alloy by the Q' and θ' precipitates. The present alloy agreed well with the previous reported Al–Si–Cu–Mg alloys regarding the cooperative strengthening by the Q' and θ' precipitates. The Q' precipitate was reported in lath shape, and the θ' precipitate was reported in plate shape [31]. It has been confirmed that the ordered metastable θ' and Q' precipitates could impart excellent strengthening effect of the α–Al matrix and provide a high yield strength of 300MPa [24,32]. The θ' precipitate in the present T6 heat–treated alloy is less than 5 nm in thickness and 50–70 nm in length , and it has coherent interfaces with the matrix, as shown in Fig. 11(a). The

Q' precipitate in the present T6 heat–treated alloy is ~6 nm in thickness and 50–70 nm in length. The fine nanoscale Q' and θ' precipitates contribute to the high yield strength of above 320 MPa of the present alloy after T6 heat treatment.

3.4. Fracture morphology

Fig. 12(a) shows the macroscopic fracture surface of the as–cast AlSiCuMgMn alloy tensile bar processed by HPDC. Fig. 12(b) shows the enlarged micrograph of Fig. 12(a), and the defect of gas pore with round shape was observed on the fracture surface, indicating the gas porosity, which was attributed to the entrapment of air under the high speed shot of HPDC. No shrinkage porosity with irregular shape was found on the fracture surface. Fig. 12(c) shows the fracture morphology in the non–defect area of the as–cast AlSiCuMgMn alloy processed by HPDC, and Fig. 12(d) shows the enlarged micrograph of Fig. 12(c). No crack initiation was found in the non–defect area of the fracture. It was reported that the ductility of the alloys with defect present was determined by the size and area fraction of defect on the fracture surface [33–36]. Thus the fracture of the as–cast AlSiCuMgMn alloy processed by HPDC was controlled by the gas porosity on the fracture surface.

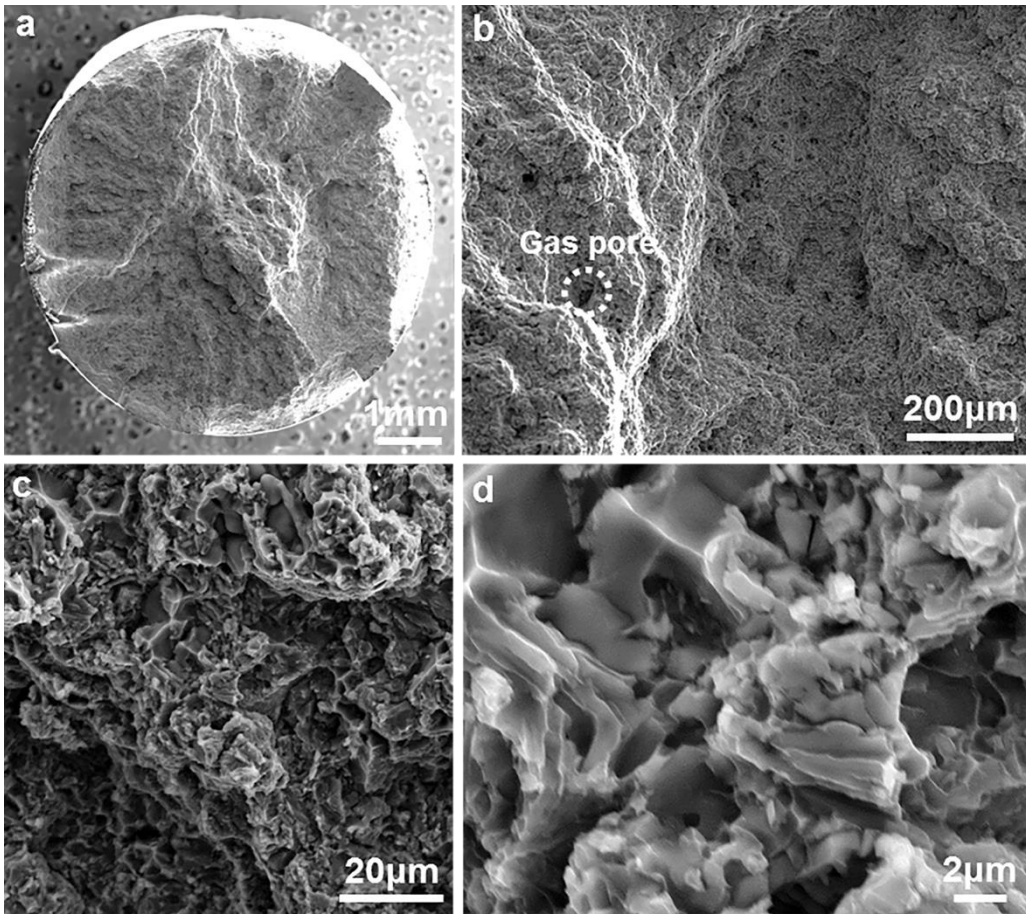

Fig. 12. SEM morphology of the fracture surface of the as–cast AlSiCuMgMn alloy processed by high pressure die casting, (a) macroscopic fracture of the tensile bar, (b) gas pores on the fracture surface, (c,d) the enlarged fracture surface.

Fig. 13(a) shows the macroscopic fracture surface of the AlSiCuMgMn alloy tensile bar processed by HPDC, after T6 heat treatment. The defect of gas pore was also observed on the fracture surface of the T6 heat–treated alloy, as indicated by the dashed circle in Fig. 13(b). The round shape of the enlarged morphology of the pore shown in Fig. 13(c) indicates that

the pore is the gas porosity. The presence of the defect of gas porosity on the fracture surface of the T6 heat–treated alloy was due to the entrapment of air in the as–cast alloy under the high speed shot of HPDC, and the gas porosity was kept after T6 heat treatment. Similar to the as–cast alloy, shrinkage porosity was also not observed in the T6 heat–treated alloy, and it was beneficial to ductility since irregular shaped shrinkage porosity was prone to crack by stress concentration. Fig. 13(d) shows the fracture morphology in the non–defect area of the T6 heat–treated alloy, and it comprises uniform distributed Al dimples and cracked Si [26], indicating the ductile fracture. According to [33–36], the fracture of the T6 heat–treated alloy is also attributed to the fine gas porosity on the fracture surface. The spheroidisation of the brittle Si phase and the solution of the brittle grain boundary intermetallic phases into the Al matrix lead to the significant increase of ductility by 41 % in the T6 heat–treated alloy over the as–cast alloy. The fine grain size of the matrix α–Al phase under the high cooling rate of HPDC, the fine size of gas porosity and the avoiding of shrinkage porosity in the alloy under HPDC, and the spheroidisation of the brittle eutectic Si phase and the solution of the brittle grain boundary intermetallic phases into the Al matrix during solution treatment result in the high ductility of the alloy after T6 heat treatment.

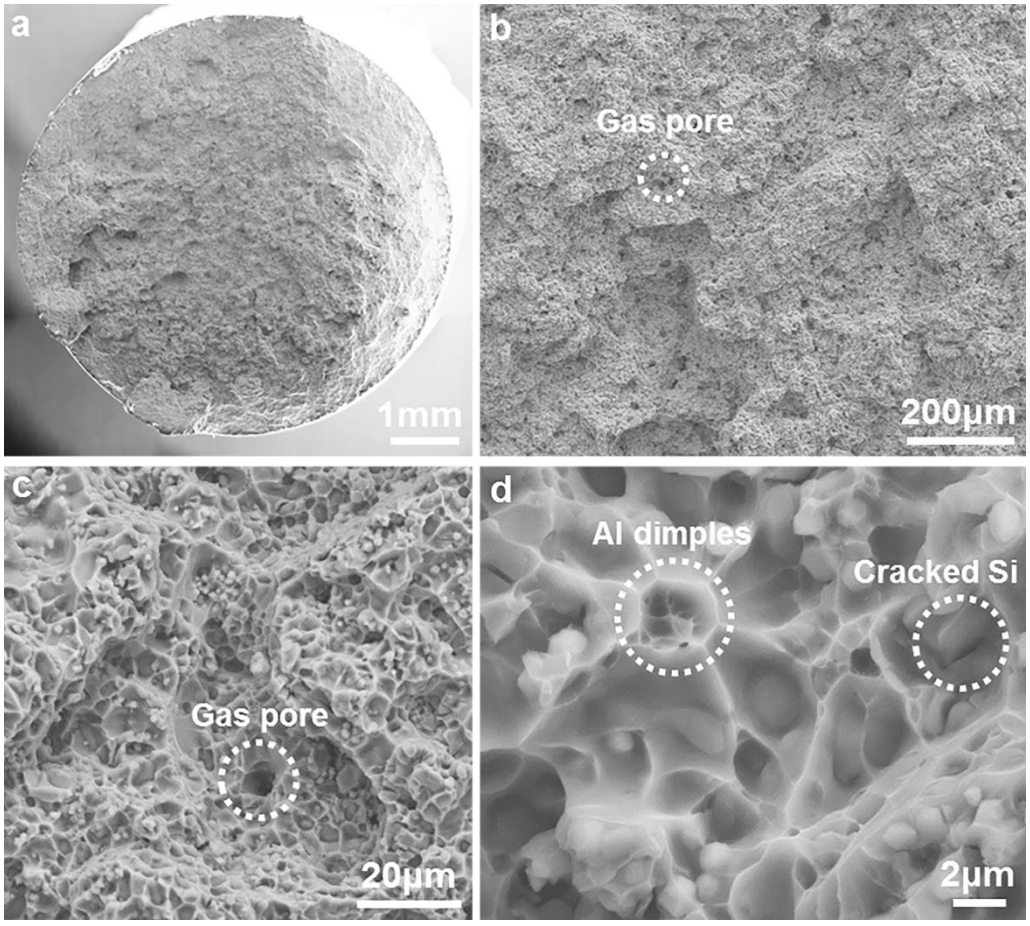

Fig. 13. SEM morphology of the fracture surface of the AlSiCuMgMn alloy processed by high pressure die casting after T6 heat treatment, (a) macroscopic fracture of the tensile bar, (b) gas pores on the fracture surface, (c,d) the enlarged fracture surface.

4. Conclusions

(1) Die–cast AlSiCuMgMn alloy containing 8.8wt.%Si, 1.7wt.%Cu, 0.4wt.%Mg and 0.5wt%Mn was developed. The tensile properties of the alloy under as–cast condition are 189 MPa of yield strength, 372 MPa of ultimate tensile strength, and 8.0 % of elongation. The tensile properties of the alloy are 211 MPa of yield strength, 391 MPa of ultimate tensile strength, and 20.7 % of elongation, after solution treatment.

(2) The AlSiCuMgMn die–cast alloy can provide the high yield strength of 321 MPa, the high ultimate tensile strength of 425 MPa and the high tensile elongation of 11.3 %, after solution and ageing treatment. The alloy demonstrates 150 % increase in ductility over the reported most advanced die–cast aluminium alloy, also comparable tensile properties to the 6000 series wrought aluminium alloys but with much lower manufacturing cost.

(3) The as–cast AlSiCuMgMn die–cast alloy mainly contains the primary α_1–Al phase solidified in the shot sleeve, the secondary α_2–Al phase solidified in the die cavity, the Al–Si eutectic phase and the intermetallic phases Q–$Al_5Cu_2Mg_8Si_6$ and θ–Al_2Cu. The Q and θ phases are dissolved into the α–Al matrix after solution, and nanoscale precipitates Q' and θ' are precipitated from the α–Al matrix for the strengthening of the alloy after ageing. Multiple effects result in the high ductility of the alloy after heat treatment.

Acknowledgements

Financial support from Innovate UK under project 131817 is gratefully acknowledged.

References

[1] L. Wang, M. Makhlouf, D. Apelian, Aluminium die casting alloys: alloy composition, microstructure, and properties-performance relationships, Int. Mater. Rev. 40 (1995) 221–238.

[2] S.X. Ji, W.C. Yang, F. Gao, D. Watson, Z.Y. Fan, Effect of iron on the microstructure and mechanical property of Al–Mg–Si–Mn and Al–Mg–Si diecast alloys, Mater. Sci. Eng. A 564 (2013) 130–139.

[3] X.X. Dong, L.J. He, X.S. Huang, P.J. Li, Effect of electromagnetic transport process on the improvement of hydrogen porosity defect in A380 aluminum alloy, Int. J. Hydrogen Energy 40 (2015) 9287–9297.

[4] X.X. Dong, X.S. Huang, L.H. Liu, L.J. He, P.J. Li, A liquid aluminum alloy electromagnetic transport process for high pressure die casting, J. Mater. Process. Technol. 234 (2016) 217–227.

[5] X.X. Dong, L.J. He, X.S. Huang, P.J. Li, Coupling analysis of the electromagnetic transport of liquid aluminum alloy during casting, J. Mater. Process. Technol. 222 (2015) 197–205.

[6] L.H. Wang, P. Turnley, G. Savage, Gas content in high pressure die castings, J. Mater. Process. Technol. 211 (2011) 1510–1515.

[7] X. Li, S.M. Xiong, Z. Guo, Correlation between porosity and fracture mechanism in high pressure die casting of AM60B alloy, J. Mater. Sci. Technol. 32 (2016) 54–61.

[8] X.X. Dong, L.J. He, X.S. Huang, P.J. Li, Effect of electromagnetic transport process on the improvement of hydrogen porosity in A380 aluminum alloy, Int J Hydrogen Energy 40 (2015) 9287–9297.

[9] G. Mrówka-Nowotnik, J. Sieniawski, A. Nowotnik, Effect of heat treatment on tensile and fracture toughness properties of 6082 alloy, J. Acheiv. Mater. Manuf. Eng. 32 (2009) 162–170.

[10] F. Ozturk, A. Sisman, S. Toros, S. Kilic, R.C. Picu, Influence of aging treatment on mechanical properties of 6061 aluminum alloy, Mater. Des. 31 (2010) 972–975.

[11] Z.X. Wang, H. Li, F.F. Miao, B.J. Fang, R.G. Song, Z.Q. Zheng, Improving the strength and ductility of Al–Mg–Si–Cu alloys by a novel thermo-mechanical treatment, Mater. Sci. Eng. A 607 (2014) 313–317.
[12] V. Kumar, D. Kumar, Investigation of tensile behaviour of cryorolled and room temperature rolled 6082 Al alloy, Mater. Sci. Eng. A 691 (2017) 211–217.
[13] S.X. Ji, F. Yan, Z.Y. Fan, Development of a high strength Al–Mg_2Si–Mg–Zn based alloy for high pressure die casting, Mater. Sci. Eng. A 626 (2015) 165–174.
[14] Z.Q. Hu, L. Wan, S.S. Wu, H. Wu, X.Q. Liu, Microstructure and mechanical properties of high strength die-casting Al–Mg–Si–Mn alloy, Mater. Des. 46 (2013) 451–456.
[15] P. Zhang, Z.M. Li, B.L. Liu, W.J. Ding, L.M. Peng, Improved tensile properties of a new aluminum alloy for high pressure die casting, Mater. Sci. Eng. A 651 (2016) 376–390.
[16] P. Zhang, Z.M. Li, B.L. Liu, W.J. Ding, Effect of chemical compositions on tensile behaviors of high pressure die-casting alloys Al-10Si-yCu-xMn-zFe, Mater. Sci. Eng. A 661 (2016) 198–210.
[17] Q.Y Hu, H.D. Zhao, F.D. Li, Microstructures and properties of SiC particles reinforced aluminum–matrix composites fabricated by vacuum–assisted high pressure die casting, Mater. Sci. Eng. A 680 (2017) 270–277.
[18] L. Wan, Z.Q. Hu, S.S.Wu, X.Q. Liu, Mechanical properties and fatigue behavior of vacuum–assist die cast AlMgSiMn alloy, Mater. Sci. Eng. A 576 (2013) 252–258.
[19] X.P. Niu, B.H. Hu, I. Pinwill, H. Li, Vacuum assisted high pressure die casting of aluminium alloys, J. Mater. Process. Technol. 105 (2000) 119–127.
[20] H.X. Cao, M.Y. Hao, C. Shen, P. Liang, The influence of different vacuum degree on the porosity and mechanical properties of aluminum die casting, Vacuum 146 (2017) 278–281.
[21] X.Y. Shi, D.J. Li, A.A. Luo, B. Hu, L. Li, X.Q. Zeng, W.J. Ding, Microstructure and mechanical properties of Mg–7Al–2Sn alloy processed by super vacuum die–casting, Metall. Mater. Trans A 44A (2013) 4788–4799.
[22] X.J. Wang, S.M. Zhu, M.A. Easton, M.A. Gibson, G. Savage, Heat treatment of vacuum high pressure die cast magnesium alloy AZ91, Int J Cast Metal Res. 27 (2014) 161–166.
[23] H.L. Yang, S.X. Ji, Z.Y. Fan, Effect of heat treatment and Fe content on the microstructure and mechanical properties of die-cast Al–Si–Cu alloys, Mater. Des. 85 (2015) 823–832.
[24] H.L. Yang, S.X. Ji, W.C. Yang, Y. Wang, Z.Y. Fan, Effect of Mg level on the microstructure and mechanical properties of die–cast Al–Si–Cu alloys, Mater. Sci. Eng. A 642 (2015) 340–350.
[25] F. Yan, W.C. Yang, S.X. Ji, Z.Y. Fan, Effect of solutionising and ageing on the microstructure and mechanical properties of a high strength die-cast Al–Mg–Zn–Si alloy, Mater. Chem. Phys. 167 (2015) 88–96.
[26] X.X. Dong, Y.J. Zhang, S.X. Ji, Enhancement of mechanical properties in high silicon gravity cast AlSi9Mg alloy refined by Al3Ti3B master alloy, Mater. Sci. Eng. A 700 (2017) 291–300.
[27] X.X. Dong, S.X. Ji, Si poisoning and promotion on the microstructure and mechanical properties of Al–Si–Mg cast alloys, J Mater. Sci. 53 (2018) 7778–7792.
[28] Q. Xiao, H.Q. Liu, D.Q. Yi, D.Y. Yin, Y.Q. Chen, Y. Zhang, B. Wang, Effect of Cu content on precipitation and age-hardening behavior in Al-Mg-Si-xCu alloys, J. Alloys Compd. 695 (2017) 1005–1013.
[29] J.Y. Hwang, R. Banerjee, H.W. Doty, M.J. Kaufman, The effect of Mg on the structure and properties of type 319 aluminum casting alloys, Acta Mater. 57 (2009) 1308–1317.

[30] X.X. Dong, Y.J. Zhang, S. Amirkhanlou, S.X. Ji, High performance gravity cast Al9Si0.45Mg0.4Cu alloy inoculated with AlB_2 and TiB_2, J. Mater. Process. Technol. 252 (2018) 604–611.
[31] A. Biswas, D.J. Siegel, D.N. Seidman, Compositional evolution of Q-phase precipitates in an aluminum alloy, Acta Mater. 75 (2014) 322–336.
[32] S.C. Weakley–Bolin, W. Donlon, C. Wolverton, J.W. Jones, J.E. Allison, Modeling the age-hardening behavior of Al–Si–Cu alloys, Metall. Mater. Trans. A 35A (2004) 2407–2412.
[33] S.G. Lee, G.R. Patel, A.M. Gokhale, A.Sreeranganathan, M.F. Horstemeyer, Variability in the tensile ductility of high–pressure die–cast AM50 Mg–alloy, Scr. Mater. 53 (2005) 851–856.
[34] S.G. Lee, G.R. Patel, A.M. Gokhale, A. Sreeranganathan, M.F. Horstemeyer, Quantitative fractographic analysis of variability in the tensile ductility of high–pressure die–cast AE44 Mg–alloy, Mater. Sci. Eng. A 427 (2006) 255–262.
[35] M.K. Surappa, E.W. Blank, J.C. Jaquet, Effect of macro–porosity on the strength and ductility of cast Al–7Si–0.3Mg alloy, Scr. Metall. 20 (1986) 1281–1286.
[36] C.H. Cáceres, B.I. Selling, Casting defects and the tensile properties of an Al–Si–Mg alloy, Mater. Sci. Eng. A 220 (1996) 109–116.